



**Efficient extraction of inorganic selenium from water by a Zr metal–organic framework: investigation of volumetric uptake capacity and binding motifs**

Journal:	<i>CrystEngComm</i>
Manuscript ID	CE-ART-06-2018-000992.R1
Article Type:	Paper
Date Submitted by the Author:	20-Jul-2018
Complete List of Authors:	Drout, Riki; Northwestern University, Department of Chemistry Howarth, Ashlee; Concordia University, Department of Chemistry and Biochemistry Otake, Ken-ichi; Northwestern University, Department of Chemistry Islamoglu, Timur; Northwestern University, Department of Chemistry Farha, Omar; Northwestern University, Department of Chemistry



Journal Name

ARTICLE

## Efficient extraction of inorganic selenium from water by a Zr metal–organic framework: investigation of volumetric uptake capacity and binding motifs

Received 00th January 20xx,  
Accepted 00th January 20xx

DOI: 10.1039/x0xx00000x

www.rsc.org/

Riki J. Drout,<sup>a</sup> Ashlee J. Howarth,<sup>b</sup> Ken-ichi Otake,<sup>a</sup> Timur Islamoglu,<sup>a</sup> and Omar K. Farha<sup>a, c, d\*</sup>

Strict monitoring and control of selenium concentrations in freshwater supplies is critical to safeguarding human health and aquatic life. A handful of previously investigated sorbents exhibit noteworthy gravimetric ( $\text{mg g}^{-1}$ ) Se uptake capacities; however, often display insufficient volumetric ( $\text{mg cm}^{-3}$ ) capacities, thereby requiring large volumes of material for commercial implementation. In pursuit of mitigating this material inefficiency, we investigated the selenite ( $\text{SeO}_3^{2-}$ ) and selenate ( $\text{SeO}_4^{2-}$ ) affinity of MOF-808, a Zr-based metal–organic framework with a high density of potential Se oxyanion binding sites. MOF-808 recorded exceptional volumetric and gravimetric Se oxyanion capacities of  $133 \text{ mg g}^{-1}$  ( $127 \text{ mg cm}^{-3}$ ) and  $118 \text{ mg g}^{-1}$  ( $112 \text{ mg cm}^{-3}$ ) for aqueous selenite and selenate, respectively. Single-crystal X-ray diffraction studies revealed that selenite and selenate can bind at the MOF node via two distinct binding motifs, an  $\eta_2\mu_2$  motif in which the oxyanion coordinates to two different metal atoms in a single node, and a  $\mu_2$  motif in which the oxyanion interacts with only a single metal atom. Furthermore, powder X-ray diffraction (PXRD) patterns and  $\text{N}_2$  adsorption/desorption isotherms confirm the retention of bulk crystallinity and porosity after the uptake of Se oxyanions.

### Introduction

In the preceding decades, researchers have uncovered the vital role of selenium as an essential trace element for human life. Selenium, of all trace essential elements, displays the most confined window of exposure between dietary deficiency ( $<40 \text{ }\mu\text{g/day}$ ) and selenosis, acute Se toxicity, ( $>400 \text{ }\mu\text{g/day}$ ).<sup>1</sup> As such, the rigid maintenance of the selenium concentration in drinking water is paramount. Selenium, which is present naturally in rocks, coal, and soil, can enter the freshwater supply via erosion.<sup>2, 3</sup> Several anthropogenic activities such as coal and fossil fuel combustion, mining, and metal refining, further increase the degree of selenium contamination in freshwater supplies.<sup>2, 3</sup> To protect both aquatic and human health, the U.S. Environmental Protection Agency (EPA) has mandated a maximum contaminant level (MCL) of 50 ppb selenium in drinking water.<sup>4</sup> While organoselenides exist, most selenium pollution remediation efforts focus on capturing

inorganic selenium species including selenite ( $\text{SeO}_3^{2-}$ ) and selenate ( $\text{SeO}_4^{2-}$ ) because their high solubility enhances their bioavailability and thereby increases the risk of exposure.<sup>2</sup>

Several strategies to remove selenite and selenate from aqueous media have been investigated including chemical reduction,<sup>5</sup> bioremediation using bacteria and fungi,<sup>6–10</sup> and adsorption.<sup>11–13</sup> Unfortunately, immense startup expenses and continuing operational costs have forestalled the large-scale use of bioremediation techniques.<sup>10</sup> Conversely, implementation of sorbent-based water decontamination technologies in industry is often impeded by insufficient uptake capacities presumed to partially result from low porosity and binding site density. Industrial application obligates that a technique be both financially lucrative and demonstrate exceptional uptake, both gravimetrically ( $\text{mg g}^{-1}$ ) and volumetrically ( $\text{mg cm}^{-3}$ ).<sup>14</sup>

<sup>a</sup> Department of Chemistry, Northwestern University, 2145 Sheridan Road, Evanston, Illinois 60208-3113, United States.

<sup>b</sup> Department of Chemistry and Biochemistry, Concordia University, 7141 Sherbrooke St. W. Montreal, Quebec, Canada, H4B 1R6.

<sup>c</sup> Department of Chemical and Biological Engineering, Northwestern University, 2145 Sheridan Road, Evanston, Illinois 60208-3113, United States.

<sup>d</sup> Department of Chemistry, Faculty of Science, King Abdulaziz University, Jeddah, Saudi Arabia.

Electronic Supplementary Information (ESI) available: CCDC 1843055, 1843056. For ESI [experimental details, adsorption capacity data, PXRD patterns, nitrogen isotherms, and SEM images] and crystallographic data in CIF or other electronic format see DOI: 10.1039/x0xx00000x

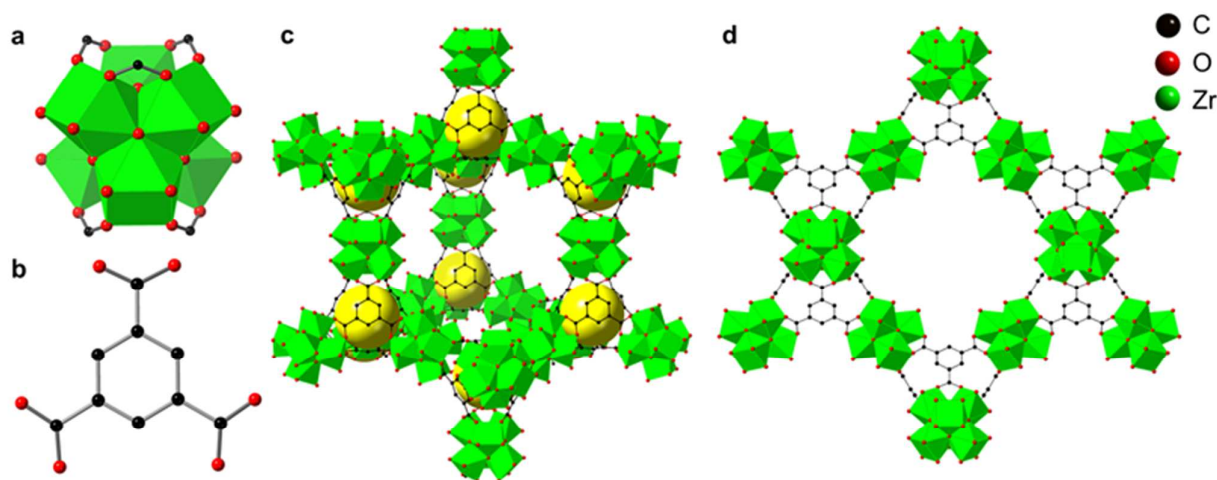


**Figure 1.** MOF-808 is comprised of a)  $Zr_6$ -nodes and b) tritopic trimesic acid linkers. The framework consists of c) large adamantane cages and exhibits the d) **spn** topology.

Metal–organic frameworks (MOFs) integrate the properties of ideal sorbents, namely high porosity, surface area, and binding site density, and have already demonstrated promise in removing toxic species from aqueous media.<sup>15–20</sup> MOFs are crystalline, multidimensional lattices comprised of inorganic metal oxide nodes and organic multitopic ligands assembled through coordination bonds.<sup>21, 22</sup> Judicious selection of the node and linker during synthesis has yielded materials displaying an extensive array of chemical and physical properties.<sup>23, 24</sup> Additionally, post-synthetic modification techniques can further tailor MOF properties through installation of chemical functionality at the nodes or linkers or by doping the framework pores.<sup>25</sup> The vast assortment of chemical and physical properties expressed by MOFs has prompted their application in gas storage<sup>26, 27</sup> and separation,<sup>28, 29</sup> catalysis,<sup>30</sup> chemical sensing,<sup>31</sup> drug delivery,<sup>32</sup> and water remediation.<sup>16, 33</sup>

Howarth *et al.* reported that NU-1000, an 8-connected MOF composed of  $Zr_6$ -based nodes and tetratopic  $H_4TBAPy$  linkers, exhibits exceptional gravimetric uptake of both selenite (95 mg  $g^{-1}$ ) and selenate (85 mg  $g^{-1}$ ).<sup>34</sup> Unfortunately, the corresponding volumetric uptake capacities are merely 45 mg  $cm^{-3}$  and 40 mg  $cm^{-3}$ , meaning that a substantial volume of material (i.e. larger column) would be required for water treatment. We anticipated that by increasing the density of potential binding sites, through use of a smaller linker and thus higher density MOF, we should increase the volumetric uptake capacities of the Se oxyanions. Herein, we investigate both the gravimetric and volumetric uptake capacities of selenite and selenate in MOF-808. This MOF, comprised of 6-connected  $Zr_6$ -based nodes and tritopic trimesic acid linkers, has smaller pores ( $\sim 17$  Å) compared to NU-1000 ( $\sim 30$  Å and 10 Å) and a higher density (0.955 g  $cm^{-3}$  vs. 0.473 g  $cm^{-3}$ ) and should thereby exhibit a higher volumetric Se uptake capacity given that the pores are still large enough to permit diffusion of the Se oxyanions (Fig. 1). Furthermore, we capitalize on the

crystalline nature of the MOF to characterize the selenite/selenate binding motif via single-crystal X-ray diffraction.

## Results and Discussion

### Preliminary Investigation of $SeO_3^{2-}$ and $SeO_4^{2-}$ Uptake

Initial experiments were performed to garner an understanding of the affinity of MOF-808 for selenite ( $SeO_3^{2-}$ ) and selenate ( $SeO_4^{2-}$ ). MOF-808 samples were exposed to aqueous solutions with  $SeO_3^{2-}$  or  $SeO_4^{2-}$  concentrations corresponding to 2 – 7 ions per  $Zr_6$ -node with Se concentrations of 61 ppm to 212 ppm. After 24 h, MOF-808 was found to capture up to 1.6  $SeO_3^{2-}$  and 1.4  $SeO_4^{2-}$  ions per  $Zr_6$ -node. These promising results prompted us to further investigate the kinetics and capacity of  $SeO_3^{2-}$  and  $SeO_4^{2-}$  uptake in MOF-808.

### Examination of Uptake Kinetics

Large scale sorbent use requires a material rapidly capture the target species. To examine the kinetics of  $SeO_3^{2-}$  and  $SeO_4^{2-}$  uptake in MOF-808, we exposed MOF-808 samples to aqueous selenite and selenate solutions with Se concentrations ranging from 15 ppm to 71 ppm corresponding to 0.5, 1.0, 1.5, 2.0, and 2.5 ions per MOF node. To monitor the adsorption of Se oxyanions by MOF-808, an aliquot of the supernatant was removed after 5, 10, 15, 30, 60, 90, and 120 min. The amount  $q$  in mg of Se oxyanion per gram of MOF-808 was determined using eq 1

$$q = (C_i - C_f)V/m \quad (1)$$

where  $C_i$  is the initial concentration (mg/L) of Se oxyanion in the solution exposed to MOF-808,  $C_f$  is the final Se oxyanion concentration (mg/L) after exposure to MOF-808,  $V$  is the

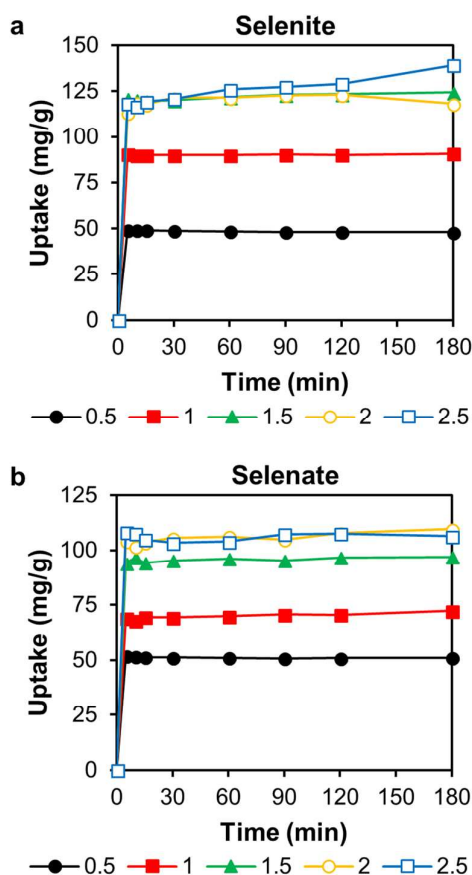


**Figure 2.** Uptake isotherms of aqueous a) selenite and b) selenate at various exposure concentrations corresponding to 0.5, 1.0, 1.5, 2.0, and 2.5 ions per node.

volume of solution exposed to MOF-808, and  $m$  is the mass (g) of MOF-808. By monitoring  $q$  as a function of time, adsorption isotherms could be constructed for each exposure concentration (Fig. 2). These isotherms reveal that within 5 min, MOF-808 reaches its maximum Se oxyanion uptake. We attribute the rapid capture kinetics to the framework's large pores ( $\sim 17$  Å) and the substitutionally labile water ( $-\text{OH}_2$ ) and hydroxyl ( $-\text{OH}$ ) groups on the MOF node.

#### Determination of Gravimetric and Volumetric Uptake Capacity

In addition to rapid kinetics, it is also critical that a material exhibit high uptake capacity for the target contaminant. Predominantly, gravimetric uptake capacities (mg/g) are reported; however, commercial application requires exceptional volumetric uptake capacities to minimize the size of purification columns. To this end, we evaluated both the gravimetric and volumetric uptakes capacities of  $\text{SeO}_3^{2-}$  and  $\text{SeO}_4^{2-}$  in MOF-808. The Type I shape of the Se sorption isotherms prompted us to employ a Linear Type I Langmuir Fit to determine the maximum uptake capacities (Figs. S2 and S3 and Table S5). MOF-808 recorded gravimetric uptake capacities of  $133 \text{ mg g}^{-1}$  and  $118 \text{ mg g}^{-1}$  for  $\text{SeO}_3^{2-}$  and  $\text{SeO}_4^{2-}$ ,

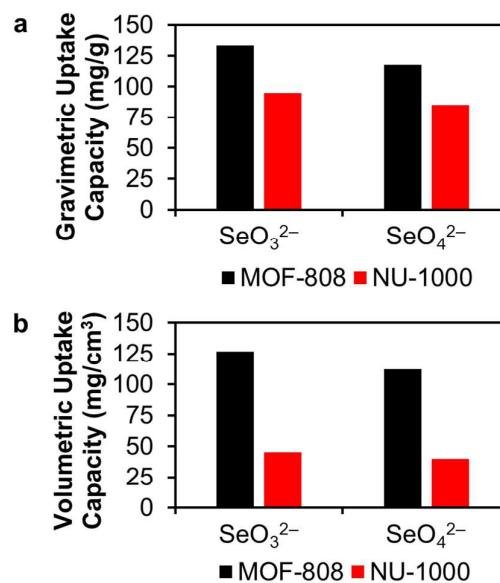


**Figure 3.** Selenite (Se(IV)) and selenate (Se(VI)) a) gravimetric uptake capacities and b) volumetric uptake capacities in MOF-808 and NU-1000.

respectively. The corresponding volumetric uptake capacities for selenite and selenate are  $127 \text{ mg cm}^{-3}$  and  $112 \text{ mg cm}^{-3}$ , respectively. These capacities are exceptional in comparison to other materials, and also noteworthy given that many materials exhibit a high affinity for only one of either selenite and selenate (Table S8).<sup>13, 35-42</sup> Furthermore, we see that MOF-808 records *higher* gravimetric and volumetric capacities for  $\text{SeO}_3^{2-}$  and  $\text{SeO}_4^{2-}$  than NU-1000 as initially predicted (Fig 3 and Tables S6 and S7).

#### Crystallographic Investigation of Binding Motifs

The amorphous nature of many commonly used sorbents renders them difficult to characterize throughout a sorption process. Advantageously, MOF crystallinity offers a unique opportunity to investigate the ion binding motifs via single-crystal X-ray diffraction analysis. To this end, single crystals of Hf-MOF-808 were prepared and analyzed after exposure to an aqueous solution of  $\text{SeO}_3^{2-}$  and  $\text{SeO}_4^{2-}$ . The Hf derivative, which exhibits a PXRD pattern and  $\text{N}_2$  adsorption/desorption isotherm shape consistent with Zr-MOF-808, was utilized to improve the quality of the single-crystal X-ray diffraction measurement.<sup>43</sup>

Both selenite and selenate were observed to bind at the  $\text{Hf}_6$ -node via two distinct motifs. In the first, an  $\eta_2\mu_2$  motif directed into the large cages, two oxygen atoms of selenite bind to two different Hf atoms within a single node (Fig. 4a and 4b). The Se–O(node) bond lengths of 1.684 Å and 1.826 Å suggest a slight distortion of the selenite ion upon binding in comparison to the accepted selenite Se–O bond length of 1.709 Å.<sup>44</sup> The O(node)–Se–O(node) bond angle of  $111.7^\circ$  is slightly larger than the accepted  $107^\circ$  for an ideal trigonal pyramid. Due to

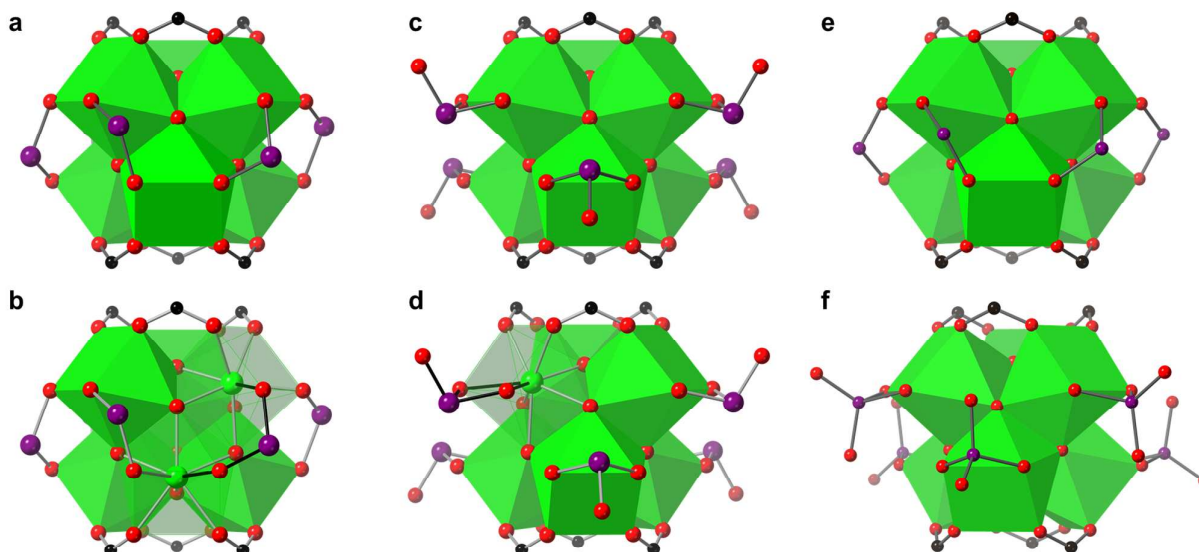


**Figure 4.** Visualizations of selenite and selenate binding at the Hf-MOF-808 node. a) Selenite  $\eta_2\mu_2$  binding motif in which two of selenite oxygen atoms coordinate to two different Hf atoms of a single node. Due to disorder, the terminal oxygen atom could not be resolved. b) Selenite  $\eta_2\mu_2$  with two transparent Hf polyhedrons to demonstrate binding to two different Hf atoms. c) Selenite  $\mu_2$  binding motif in which two oxygen atoms coordinate the same Hf atom in the node. d) Selenite  $\mu_2$  binding motif with transparent Hf polyhedron to demonstrate binding at a single Hf atom. e) Selenate  $\eta_2\mu_2$  binding motif. f) Selenate  $\mu_2$  binding motif. The green, red, black, and purple spheres represent Hf, O, C, and Se atoms, respectively.

the disorder and low occupancy of this binding motif, the terminal oxygen atom could not be resolved.<sup>45</sup> Selenite can also bind to the node via a  $\mu_2$  motif directed into the cage in which two of the selenite oxygen atoms coordinate to a single Hf atom (Fig. 4c and 4d). The Se–O(node) and the Se–O(terminal) bond lengths are 1.853 Å and ~1.727 Å, respectively. The slight elongation of the bonds may be due to the binding event itself or the disordered nature of the binding event. The bond angles of 89.99° and 101.9° for O(node)–Se–O(node) and O(node)–Se–O(terminal) also suggest significant distortion of the ion upon binding.

Similarly, selenate ( $\text{SeO}_4^{2-}$ ) binds via both  $\eta_2\mu_2$  and  $\mu_2$  motifs. In the  $\eta_2\mu_2$  motif, the Se–O(node) bond lengths are 1.610 Å and 1.669 Å (Fig. 4e) and are moderately consistent with the 1.64 Å Se–O bond length recorded for hydrated selenate in aqueous media.<sup>44</sup> The O(node)–Se–O(node) bond angle is 117.6°, larger than anticipated (109.5°) for an ideal tetrahedral ion. In comparison, the Se–O(node) bond lengths of the  $\mu_2$  motif are significantly elongated to 1.767 Å; however, the Se–O(terminal) bond lengths of 1.603 Å and 1.649 Å are consistent (Fig. 4f). The O(node)–Se–O(node) bond angle is significantly contracted to 92.39° possibly as a result of the aforementioned Se–O(node) bond elongation. The bond angles between terminal and node-based oxygen atoms differ only slightly from the ideal tetrahedral bond angle.

The majority of the bound selenite was found in the  $\mu_2$  motif (69%) in comparison to the  $\eta_2\mu_2$  motif (31%). Similarly, selenate primarily binds via the  $\mu_2$  motif (75%) suggesting that coordinating to a single Hf atom is more stable as compared to

coordinating to two Hf atoms in the  $\eta_2\mu_2$  motif (25%). We suspect this favorability stems from the distribution of terminal hydroxyl and water groups on the node and charge balancing requirements; however, the proton topology of MOF-808 requires further investigation.<sup>46</sup>

#### Post-Adsorption Characterization

To confirm the retention of crystallinity and porosity, selenite- and selenate-loaded MOF-808 samples were fully characterized. As monitored by ICP-OES, no zirconium leaching was observed during the sorption process. Powder X-ray diffraction (PXRD) patterns verify that bulk purity and crystallinity of MOF-808 are preserved during the sorption of selenite and selenate (Fig. S4). Nitrogen adsorption/desorption isotherms for native MOF-808 and MOF-808 loaded with selenite or selenate are nearly identical in shape and yield Brunauer–Emmett–Teller (BET) surface areas of 1930 m<sup>2</sup> g<sup>-1</sup> (1840 m<sup>2</sup> cm<sup>-3</sup>), 1680 m<sup>2</sup> g<sup>-1</sup> (1880 m<sup>2</sup> cm<sup>-3</sup>), and 1790 m<sup>2</sup> g<sup>-1</sup> (2010 m<sup>2</sup> cm<sup>-3</sup>), respectively (Fig. S5). The observed decrease in gravimetric surface area is consistent with the increase of the framework mass when chemical moieties are captured or installed at the MOF node.<sup>34, 47, 48</sup> Additionally, the associated pore size distributions further support the capture of  $\text{SeO}_3^{2-}$  and  $\text{SeO}_4^{2-}$  at the MOF node (Fig. S6). Finally, scanning electron microscopy (SEM) images and the associated energy dispersive X-ray spectroscopy (EDS) spectra verify the uniform distribution of Se throughout MOF-808 crystals exposed to aqueous selenite and selenate solutions (Fig. S7).

## Conclusions

In summary, the suitability of MOF-808 as a sorbent for selenite and selenate was thoroughly investigated. Post-adsorption characterization of MOF-808 loaded with selenite and selenate confirms the framework retains its crystallinity and porosity throughout the uptake process. Notably, MOF-808 was found to have exceptional gravimetric and volumetric Se oxyanion uptake capacities of  $133 \text{ mg g}^{-1}$  ( $127 \text{ mg cm}^{-3}$ ) and  $118 \text{ mg g}^{-1}$  ( $112 \text{ mg cm}^{-3}$ ) for  $\text{SeO}_3^{2-}$  and  $\text{SeO}_4^{2-}$ , respectively. Additionally, diffusion is facilitated by the framework pores and results in rapid saturation in <5 min. Furthermore, single-crystal X-ray diffraction studies reveal that selenite and selenate both coordinate at the MOF node via two distinct binding motifs. In the  $\eta_2\mu_2$  motif, the ion binds through two oxygen atoms to two Hf atoms in the node; whereas, in the  $\mu_2$  motif, the Se oxyanion oxygen atoms are bound to a single Hf atom in the node. We are hopeful that the exceptional volumetric Se uptake capacity and the illuminating crystallographic investigation reported here will prompt researchers to thoroughly examine the potential of MOFs in the water decontamination effort.

## Conflicts of interest

There are no conflicts to declare.

## Acknowledgements

The authors are grateful for the financial support from the U.S. Department of Energy, Nuclear Security Administration under Award Number DE-NA0003763 and Northwestern University. ICP-OES metal analysis was performed at the Northwestern University Quantitative Bio-element Imaging Center. X-ray crystallographic investigations were performed at Northwestern University in the IMSERC facility, which is supported by the Soft and Hybrid Nanotechnology Experimental (SHyNE) Resource (NSF ECCS-1542205), the State of Illinois, and the International Institute of Nanotechnology (IIN).

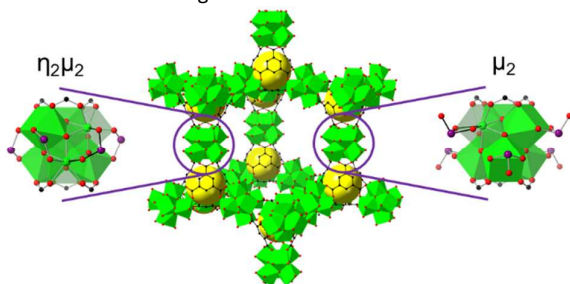
## References

- W. H. Organization, *WHO chronicle*, 2011, **38**, 104-108.
- W. H. Organization, *WHO/HSE/WSH/10.01/14*, 2011.
- A. D. Lemly, *Ecotoxicology and Environmental Safety*, 2004, **59**, 44-56.
- U. S. E. P. Agency, *EPA 816-F-09-004*, 2009.
- A. P. Murphy, *Industrial & Engineering Chemistry Research*, 1988, **27**, 187-191.
- M. Khalilian, M. R. Zolfaghari and M. Sole, *Report of Health Care*, 2015.
- M. Khalilian, M. R. Zolfaghari and M. Soleimani, *Iranian journal of microbiology*, 2015, **7**, 94.
- U. Martin, B. Katarina, B. Marek and M. Peter, *CLEAN – Soil, Air, Water*, 2016, **44**, 610-614.
- D. Adriano, W. Wenzel, J. Vangronsveld and N. Bolan, *Geoderma*, 2004, **122**, 121-142.
- L. Wu, *Ecotoxicology and environmental safety*, 2004, **57**, 257-269.
- D. Peak, *Journal of colloid and interface science*, 2006, **303**, 337-345.
- G. Jegadeesan, K. Mondal and Lalvani, *Environmental Technology*, 2005, **26**, 1181-1188.
- J. S. Yamani, A. W. Lounsbury and J. B. Zimmerman, *Water Research*, 2014, **50**, 373-381.
- M. A. Shannon, P. W. Bohn, M. Elimelech, J. G. Georgiadis, B. J. Marinas and A. M. Mayes, *Nature*, 2008, **452**, 301.
- E. M. Dias and C. Petit, *Journal of Materials Chemistry A*, 2015, **3**, 22484-22506.
- A. J. Howarth, Y. Liu, J. T. Hupp and O. K. Farha, *CrystEngComm*, 2015, **17**, 7245-7253.
- M. Kadhom and B. Deng, *Applied Materials Today*, 2018, **11**, 219-230.
- L. Siqing, C. Yifa, P. Xiaokun, Z. Shenghan, F. Xiao, Z. Junwen and W. Bo, *Chinese Journal of Chemistry*, 2016, **34**, 175-185.
- L. Zhu, D. Sheng, C. Xu, X. Dai, M. A. Silver, J. Li, P. Li, Y. Wang, Y. Wang, L. Chen, C. Xiao, J. Chen, R. Zhou, C. Zhang, O. K. Farha, Z. Chai, T. E. Albrecht-Schmitt and S. Wang, *Journal of the American Chemical Society*, 2017, **139**, 14873-14876.
- D. Sheng, L. Zhu, C. Xu, C. Xiao, Y. Wang, Y. Wang, L. Chen, J. Diwu, J. Chen, Z. Chai, T. E. Albrecht-Schmitt and S. Wang, *Environmental Science & Technology*, 2017, **51**, 3471-3479.
- H. C. Zhou, J. R. Long and O. M. Yaghi, *Chem Rev*, 2012, **112**, 673-674.
- H. Li, M. Eddaoudi, M. O'Keeffe and O. M. Yaghi, *Nature*, 1999, **402**, 276-279.
- L. Ma, J. M. Falkowski, C. Abney and W. Lin, *Nature chemistry*, 2010, **2**, 838.
- D. Yuan, D. Zhao, D. Sun and H. C. Zhou, *Angewandte Chemie International Edition*, 2010, **49**, 5357-5361.
- T. Islamoglu, S. Goswami, Z. Li, A. J. Howarth, O. K. Farha and J. T. Hupp, *Acc Chem Res*, 2017, **50**, 805-813.
- M. Eddaoudi, J. Kim, N. Rosi, D. Vodak, J. Wachter, M. O'Keeffe and O. M. Yaghi, *Science*, 2002, **295**, 469-472.
- L. J. Murray, M. Dinca and J. R. Long, *Chem Soc Rev*, 2009, **38**, 1294-1314.
- J. R. Li, R. J. Kuppler and H. C. Zhou, *Chem Soc Rev*, 2009, **38**, 1477-1504.
- K. Sumida, D. L. Rogow, J. A. Mason, T. M. McDonald, E. D. Bloch, Z. R. Herm, T. H. Bae and J. R. Long, *Chem Rev*, 2012, **112**, 724-781.
- J. Lee, O. K. Farha, J. Roberts, K. A. Scheidt, S. T. Nguyen and J. T. Hupp, *Chem Soc Rev*, 2009, **38**, 1450-1459.
- L. E. Kreno, K. Leong, O. K. Farha, M. Allendorf, R. P. Van Duyne and J. T. Hupp, *Chem Rev*, 2012, **112**, 1105-1125.
- P. Horcajada, T. Chalati, C. Serre, B. Gillet, C. Sebrie, T. Baati, J. F. Eubank, D. Heurtaux, P. Clayette, C. Kreuz, J. S. Chang, Y. K. Hwang, V. Marsaud, P. N. Bories, L. Cynober, S. Gil, G. Ferey, P. Couvreur and R. Gref, *Nat Mater*, 2010, **9**, 172-178.
- N. S. Bobbitt, M. L. Mendonca, A. J. Howarth, T. Islamoglu, J. T. Hupp, O. K. Farha and R. Q. Snurr, *Chem Soc Rev*, 2017, **46**, 3357-3385.
- A. J. Howarth, M. J. Katz, T. C. Wang, A. E. Platero-Prats, K. W. Chapman, J. T. Hupp and O. K. Farha, *J. Am. Chem. Soc.*, 2015, **137**, 7488-7494.

35. Y. T. Chan, W. H. Kuan, T. Y. Chen and M. K. Wang, *Water Research*, 2009, **43**, 4412-4420.
36. A. J. Howarth, M. J. Katz, T. C. Wang, A. E. Platero-Prats, K. W. Chapman, J. T. Hupp and O. K. Farha, *Journal of the American Chemical Society*, 2015, **137**, 7488-7494.
37. L. Zhu, L. Zhang, J. Li, D. Zhang, L. Chen, D. Sheng, S. Yang, C. Xiao, J. Wang, Z. Chai, T. E. Albrecht-Schmitt and S. Wang, *Environmental Science & Technology*, 2017, **51**, 8606-8615.
38. L. Ma, S. M. Islam, C. Xiao, J. Zhao, H. Liu, M. Yuan, G. Sun, H. Li, S. Ma and M. G. Kanatzidis, *Journal of the American Chemical Society*, 2017, **139**, 12745-12757.
39. G. Nisa, G. Mustafa and A. A. Osman, *Journal of Applied Polymer Science*, 2011, **122**, 1134-1141.
40. N. Tian, Z. Zhou, X. Tian, C. Yang and Y. Li, *Separation and Purification Technology*, 2017, **176**, 66-72.
41. Y. Toshiyuki, T. Takashi and Y. Hideaki, *Bulletin of the Chemical Society of Japan*, 2003, **76**, 2225-2232.
42. J. Li, Y. Liu, X. Wang, G. Zhao, Y. Ai, B. Han, T. Wen, T. Hayat, A. Alsaedi and X. Wang, *Chemical Engineering Journal*, 2017, **330**, 1012-1021.
43. Y. Liu, R. C. Klet, J. T. Hupp and O. Farha, *Chemical Communications*, 2016, **52**, 7806-7809.
44. L. Eklund and I. Persson, *Dalton Transactions*, 2014, **43**, 6315-6321.
45. J. Jiang, F. Gándara, Y.-B. Zhang, K. Na, O. M. Yaghi and W. G. Klemperer, *Journal of the American Chemical Society*, 2014, **136**, 12844-12847.
46. R. C. Klet, Y. Liu, T. C. Wang, J. T. Hupp and O. K. Farha, *Journal of Materials Chemistry A*, 2016, **4**, 1479-1485.
47. R. J. Drout, K. Otake, A. J. Howarth, T. Islamoglu, L. Zhu, C. Xiao, S. Wang and O. K. Farha, *Chem. Mater.*, 2018, **30**, 1277-1284.
48. S. Rangwani, A. J. Howarth, M. R. DeStefano, C. D. Malliakas, A. E. Platero-Prats, K. W. Chapman and O. K. Farha, *Polyhedron*, DOI: <https://doi.org/10.1016/j.poly.2018.05.021>.

MOF-808 displays enhanced gravimetric and volumetric uptake capacities for selenium oxyanions and the binding motifs were crystallographically characterized.

Table of Contents Figure



Entry: